HHS Public Access

Author manuscript

Behav Neurosci. Author manuscript; available in PMC 2021 December 01.

Published in final edited form as:

Behav Neurosci. 2020 December ; 134(6): 529–546. doi:10.1037/bne0000409.

'Awake delta' and theta-rhythmic hippocampal network modes during intermittent locomotor behaviors in the rat

Nathan W. Schultheiss[1], **Maximilian Schlecht**[1], **Maanasa Jayachandran**[1], **Deborah R. Brooks**[2], **Jennifer L. McGlothan**[2], **Tomás R. Guilarte**[2], **Timothy A. Allen**[1,2]

[1]Cognitive Neuroscience Program, Department of Psychology, Florida International University, Miami, FL, 33199

[2]Department of Environmental Health Sciences, Robert Stempel College of Public Health, Florida, International University, Miami, FL, 33199

Abstract

Delta-frequency network activity is commonly associated with sleep or behavioral disengagement accompanied by a dearth of cortical spiking, but delta in awake behaving animals is not well understood. We show that hippocampal (HC) synchronization in the delta frequency band (1-4 Hz) is related to animals' locomotor behavior using detailed analyses of the HC local field potential (LFP) and simultaneous head- and body-tracking data. In contrast to running-speed modulation of the theta rhythm (6-10 Hz), delta was most prominent when animals were stationary or moving slowly, i.e. when theta and fast gamma (65-120 Hz) were weak, and often developed rapidly when animals paused briefly between runs. We next combined time-frequency decomposition of the LFP with hierarchical clustering algorithms to categorize momentary estimations of the power spectral density (PSD) into putative *modes* of HC activity. Delta and theta power were strikingly orthogonal across spectral modes, as well as across bouts of precisely-defined running and stationary behavior. Delta-band and theta-band coherences between HC recording sites were monotonically related to theta-delta ratios across modes; and whereas theta coherence between HC and medial prefrontal cortex (mPFC) increased during running, delta-band coherence between mPFC and HC increased during stationary bouts. Taken together, our findings suggest that delta-dominated network modes (and corresponding mPFC-HC couplings) represent functionally-distinct circuit dynamics that are temporally and behaviorally interspersed amongst theta-dominated modes during navigation. As such, delta modes could play a fundamental role in coordinating encoding and retrieval mechanisms or decision-making processes at a timescale that segments event sequences within behavioral episodes.

Keywords

delta; theta; spectral mode; gamma; hippocampus; prefrontal cortex; locomotion; episodic memory

Corresponding Author: Timothy A. Allen, PhD, Department of Psychology, Florida International University, 11200 SW 8th Street, Miami, FL, 33199, tallen@fiu.edu, Website: http://allenlab.fiu.edu/, Twitter: @AllenNeuroLab.

Conflict of Interest: The authors declare no competing financial interests.

Introduction

Delta-frequency activity (1-4 Hz) is often observed in local field potential (LFP) recordings, but it is rarely analyzed in detail. This is in part due to the fact that during polymorphic slow-wave sleep (Steriade et al., 1993, Amzica & Steriade, 1998), delta waves correspond to periods of widespread cortical silence that encompass both principal cells and interneurons throughout cortical layers (Sirota & Buzsaki, 2005), giving the impression that neural computational processes are offline. Delta frequency activity is also evident in awake rodents (Bennett et al., 2013, Crochet & Petersen, 2006, Poulet & Petersen, 2008, Zagha et al. 2013), monkeys (Lakatos et al., 2005, Tan et al., 2014), and humans (Sachdev et al., 2015), but overt behavioral correlates of delta are lacking, and sensory stimuli or movement can elicit desynchronized states that supplant slow activity (Zagha et al. 2013, Tan et al., 2014).

During the slow oscillation of non-REM sleep, delta waves correspond to hyperpolarized down-states interspersed between hippocampal ripple-associated and plastic phases of the cortical slow oscillation (Sirota & Buzsaki, 2005, Todorova & Zugaro, 2019). Interestingly, delta activity has been shown to become increasingly prevalent during prolonged periods of wakefulness, even meriting comparison to neuroanatomically-localized sleep in awake animals (Vyazovskiy et al., 2011), and delta waves are accentuated when sleep is finally possible after such deprivation (Vyazovskiy et al., 2009). Does this amplification of delta activity somehow ameliorate prolonged or excessive neural exertion, or is it otherwise related to the continuous accumulation of waking experience without the restorative punctuation that sleep provides? An important recent study found that, rather than absolute cortical silence during delta waves, a few neurons remain active. Furthermore, neuronal ensembles active during delta waves bridge hippocampal ripple-related replay events and subsequent plastic phases of the slow oscillation supporting consolidation of memory for recent experiences prior to sleep (Todorova & Zugaro, 2019). Perhaps then, delta is not exactly a sign of cortical sleep, but rather an indication that competing cortical ensembles need to be quieted in order to draw into greater relief the specific activities of neurons representing experiences to be encoded into memory.

In contrast to delta, the theta rhythm (6-10 Hz) in (HC) and connected structures is a well-organized oscillation with well-characterized functional significance for spatial navigation and episodic memory, as well as working memory (Winson, 1978, Buzsaki, 2002, Lisman & Jensen, 2013, Buzsaki & Moser, 2013). Theta is prominent during behaviors related to active attention and environmental sampling (Aghajan et al., 2017, Barth et al., 2018), and theta frequency and power are both correlated to locomotor speed (Whishaw & Vanderworf, 1973, McFarland et al., 1975, Maurer et al., 2005, Hinman et al., 2016). Theta also exhibits functionally-relevant cross-frequency coupling to gamma oscillations (>25 Hz) (Canolty et al., 2006, Tort et al., 2009, Shirvalkar et al., 2010, Lisman & Jensen, 2013) and modulates robust spiking within HC (Okeefe & Recce, 1993, Foster & Wilson, 2007, Johnson & Redish, 2007) and its projection targets (Sirota et al., 2008, van der Meer & Redish, 2011). Theta-rhythmic temporal sculpting of spike patterns orchestrates neuronal interactions and synchrony within hippocampal populations, as well as between HC and medial prefrontal cortex (mPFC) networks responsible for aspects of learning, planning and decision making,

and neural representations of ongoing, remembered, or imagined future experiences (Richard et al., 2013, Pfeiffer & Foster, 2013, Redish, 2016, Schacter et al., 2007).

Running speed modulation of the HC theta rhythm is an integral mechanistic component of models of spatial navigation and episodic memory (Hasselmo, 2011, Buzsaki & Moser, 2013, Schultheiss et al., 2015) and reflects, in part, the integration of sensory-motor information during locomotion (Bland & Oddie, 2001). Locomotion also modulates the firing rates and patterns of individual neurons in parahippocampal structures (Kropff et al., 2015, Hinman et al., 2016) as well as primary sensory cortices; and numerous recent studies have demonstrated that desynchronized and slow-oscillatory cortical states correspond to animals' behavioral activity and quiescence, respectively (Neill & Stryker, 2010, Saleem et al., 2013, Reimer et al., 2014, Vinck et al., 2015, Zagha et al., 2013, Tan et al., 2014).

Analyses of oscillatory dynamics in HC during behavior have begun to reveal distinct operational states or 'modes' that are distinguishable in terms of the spectral content of the LFP and neuronal spiking (Barth et al., 2018, Kemere et al., 2013, Colgin, 2015, Amemiya & Redish, 2018, Zhang et al., 2019). Focusing on the delta and theta frequency bands, we asked to what extent modes of HC activity, defined by the spectral content of the HC LFP, reflect differences in network coupling and behavior. Using a combination of hierarchical clustering algorithms and time-frequency decomposition, we found that delta synchrony in HC was negatively related to speed, delta-dominated modes were orthogonal to theta modes in a manner mediated by locomotor activity, and both delta and theta modes were reflected in intrahippocampal network coupling and mPFC-HC circuit states.

Methods

Subjects.

Six adult male Long-Evans rats, weighing 600-700g at the time of surgery, were used in the study. Rats are uniquely identified in this report as "NCL0###". Rats were individually housed in a climate-controlled vivarium and maintained on a reverse 12hr light/dark cycle. Daily experiments were conducted during the dark cycle active periods. Rats had free access to food and water with the exception that food was not available during a 1-2hr period prior to each session where rewards were given. All procedures were approved by the Institutional Animal Care and Use Committee at Florida International University.

Implants.

Rats underwent surgery to implant chronic recording electrodes. Four animals were implanted for HC recordings with 32-channel silicon probes arranged as tetrodes with 25 μm between adjacent electrode sites and impedances of 1.23 ± 0.32 MΩ. The eight tetrodes were distributed across four shanks at tip-to-tetrode depths of 78 μm and 228 μm (NeuroNexus A4X2-tet-5mm). Shanks were separated by 200 μm giving each probe a total length of 0.67 cm. During implantation, the long axis was oriented medial-lateral to sample proximal CA1 and CA2 of dorsal HC. Two animals were implanted for dual-site recordings with stainless steel wire electrodes (0.42 ± 0.25 MΩ) using custom designed (Autodesk Inventor) and 3-D printed implant bodies (3D Systems ProJet 1200) to house the electrodes coupled to an

integrated electrode interface board. These implants comprised a grid of 18 electrodes targeting HC (2 x 2.5 mm footprint, 4 electrode rows, 0.5 mm center-to-center) and 14 electrodes arranged in two parallel rows (4 x 1 mm footprint, 0.5 mm long-axis spacing) aligned to the rostrocaudal axis of mPFC.

Surgical and post-operative procedures.

General anesthesia was induced with isoflurane (5%) mixed with oxygen (0.8 L/min) and maintained throughout surgery at 1-4% as needed. Body temperature was monitored throughout surgery, and a Ringer's solution (5% dextrose, 1 ml increments) was delivered at intervals of ~1 hour to maintain hydration. The hair was cut over the scalp and rats were placed in a stereotaxic device. Glycopyrulate (0.5 mg/kg, s.c.) was administered to assist respiratory stability, and ophthalmic ointment was applied to the eyes. Prior to incision, four injections of marcaine were made to the scalp (~0.1 ml, 7.5 mg/ml, s.c.). The pitch of the skull was leveled between bregma and lambda, two stainless steel ground screws were placed in the left parietal bone, and four or five titanium support screws were anchored to the skull. For silicon probe implants targeting dorsal HC, rectangular craniotomies were drilled to accommodate the probe shanks centered on coordinates A/P −3.24 mm, M/L 2.7 mm. For dual-site implants, craniotomies were shaped to accommodate the respective geometries of the electrode grids targeting HC (at A/P −2.9 mm, M/L 2.0 mm) and mPFC (A/P 3.0 mm, M/L 1.0 mm). After removal of the dura, implants were lowered on the stereotaxic arm until the electrode tips were just above the cortical surface. The ground wire was attached to the ground screws, and implants were lowered such that HC electrodes reached ~2.8 mm below the cortical surface and mPFC electrodes reached ~3.3 mm in depth. Sodium alginate was applied to the exposed surface of the brain within the craniotomy, and dental cement was applied to permanently affix the implant to the skull screws. Neosporin® was applied to the skin surrounding the implant, and flunixin (2.5 mg/kg, s.c.) was administered for analgesia. Rats were removed from the stereotaxic device and allowed to wake up and rest on a heating pad until ambulatory prior to being returned to their home cages. Neosporin® and flunixin were administered again the day following surgery, and rats were monitored closely for five days thereafter to ensure no negative symptoms emerged and that body weight was maintained. A 5-day regimen of daily Baytril injections (s.c.) was given during this time to preempt any post-surgical infection. At least one week was allowed for recovery from surgery prior to beginning experiments.

Behavioral Apparatus.

All experiments consisted of freely behaving rats in an open field environment (122 x 118 x 47 cm). The interior walls of the arena were lined with white vinyl; a custom-made white cutting board served as the floor; and all corners were sealed with white silicone. The arena was mounted on stilts 72 cm above the floor and the exterior was encased in grounded Faraday shielding. Two video cameras were used to track rats' locomotion and other behaviors with a bird's eye view. These were mounted near the ceiling, 28 cm apart from one another, 150 cm above of the midline of the arena floor, yielding ~4.6 pixel/cm resolution in recorded videos and corresponding tracking data.

The entire behavioral apparatus was enshrouded with black curtains suspended from the ceiling and extending to the floor. Small gaps at the Velcro® closures at the corners between the four curtain panels were used to observe rats covertly during recording sessions to monitor that the head-stage, cables, and elastic tethers were not tangled, and to confirm that rats were awake during periods of relative inactivity. The white arena was illuminated dimly with red light from LED strips arranged in a square and mounted at the level of the video cameras. Outside the curtains, all lights were kept off during recording sessions save the experimenter's computer monitor, which was not visible from the interior of the behavioral arena.

Electrophysiological recordings.

Throughout each experiment wide-band neural data were acquired with a Plexon OmniplexD recording system with A/D conversion at 40 kHz (16 bit). Briefly, a digital head stage processing subsystem (Intan, 32 channel) passed continuous wide-band data referenced against the ground screws (low cutoff = 0.7 Hz) to be stored on a hard drive using PlexControl data acquisition software. For local field potential (LFP) analysis, the wideband data was down-sampled to 2kHz.

Behavioral tracking.

In parallel with neural recordings, Cineplex software (Plexon) was used to track and record (30 fps) the location of two clusters of LED florets (one green and one blue) that were offset ~2 cm laterally from attachments to the head-stage at ~3 cm above the rat's head. Each LED cluster comprised three florets oriented upward and angled slightly outward. This construction reduced gaps in tracking data that could otherwise result from a variety of behaviors including rearing and grooming in which rats oriented their heads away from the level plane or otherwise obscured the LEDs.

The physical and software settings for the two video cameras used for behavioral tracking were tuned independently to provide complementary data types for subsequent offline analyses. Whereas camera one was tuned to optimize tracking of the head-mounted LEDs with high color saturation and contrast against a near-black background; camera two was tuned to (1) maximize light sensitivity (sacrificing color saturation) allowing rats' dark fur and body contours to be distinguishable against the white floor, while also (2) maintaining the ability to track the bright LED luminance peaks against the dimly illuminated environment. Raw videos from both cameras were recorded for all experiments, and online video tracking during each experiment yielded an output file for each camera containing the coordinates of the center of each LED cluster for each video frame. Video tracking frame captures were synchronized in real time to the simultaneously recorded neural data via a central timing board (Plexon).

After each experiment, the video file from camera two was retracked in Cineplex's object contour tracking mode. Body location was calculated as the center of mass from difference images obtained by subtracting an image of the empty arena (captured just prior to placing the rat on the floor inside) from each frame of the video from camera two. Movement speeds were calculated from these body coordinates.

Co-registration of LED and body tracking data.

Following acquisition, all analyses of behavioral data were performed with custom-written Matlab scripts (MathWorks, Natick, MA). First, the coordinate system for camera one was mapped onto the coordinate system for camera two for each experiment. These mappings were achieved as follows: First, we restricted the data to timepoints for which tracking data were complete (for both LEDs, both cameras, and body location) and free from identifiable tracking errors such as occasionally resulted from reflections of the LEDs on surfaces within the arena. Second, the location of the head was calculated as the midpoint between the two LED clusters for each timepoint. Next, a 3rd order polynomial function was fitted to the set of simultaneously-recorded x-coordinate pairs from the two cameras, and the same was done for the y-coordinate pairs. These two fitting functions independently defined the relationships between the x- and y-coordinates of the head on camera one to the x- and y-coordinates of the head on camera two. These mappings were then used to convert the coordinates of the LED clusters from camera one onto the coordinate system for camera two, allowing the precise LED tracking data to be integrated with the body tracking data.

We derived for each timestep the animal's head direction (HD) relative to the environment (from the axis between the two head-mounted LED clusters); body direction (BD) relative to the environment (from the midpoint between the LEDs to the center of the body); head angle (HA) relative to the body (using the LED axis relative to BD); and the rotational velocity of the body.

Definitions of locomotor and stationary bouts.

To isolate bouts of locomotion from other behaviors including grooming and rearing, we first required that movement speed be maintained above 5 cm/sec for a minimum duration of 2.05 seconds with a minimum peak speed of 15 cm/sec. We then eliminated all instances where head angle exceeded 35 degrees or body rotational velocity exceeded 52.5 degrees per second at any time. Stationary bouts were required to meet the same minimum duration, HA, and rotational criteria and not exceed a maximum movement speed of 5 cm/sec.

Rewarded behavioral sessions.

To familiarize rats with the food rewards to be used, five Fruit Loops™, broken into individual rewards of ~1/4 loop, were given daily in rats' home cages for five days prior to beginning these experiments. Subsequently, each rat was run in two or more behavioral sessions lasting ~35 minutes each during which rewards were sporadically delivered. Rats with silicon probe implants were run in two such sessions, whereas rats with wire electrode implants were run in eight. Supplemental Figures 1 & 2 show behavioral measures for each rat across successive rewarded sessions (and non-rewarded sessions). There was no explicit task in rewarded sessions, but rewards were distributed sporadically one-at-a-time throughout the arena to motivate running to retrieve specific rewards as well as exploratory foraging generally. Rewards were distributed from above onto the arena floor using PVC pipes mounted at the ceiling outside the peripheral curtain enclosure and descending to terminate centrally adjacent to the video cameras. This approach was intended to minimize rats' awareness of or attentiveness to the experimenter (which can be significant in similar behavioral paradigms using manual reward deliveries). None-the-less, some rats exhibited

'anticipatory' behaviors between reward deliveries, standing upright and fixating upward towards the reward delivery pipes.

Rats' reward-seeking behaviors, including running speeds while retrieving rewards and the consistency, speed, and total duration of foraging during a session (as well as the frequency and duration of reward-irrelative behaviors) were highly variable between individuals, between sessions (for each rat), and also within sessions (Fig. 1, and Supp. Figs. 1 & 2). Thus, the temporal pattern and number of rewards delivered per session were not predetermined. Rather, the experimenter attempted to maintain two to five rewards distributed broadly across the open field arena at a given time while rats were actively foraging. Rewards were delivered infrequently (one to two per minute) while rats were relatively idle, allowing not more than ~10 to accumulate within the environment. No rewards were delivered while rats were actively grooming.

Free exploration during non-rewarded behavioral sessions.

Rats with silicon probe implants in HC (n=4) were also run in five non-rewarded sessions giving a total of seven experimental sessions per rat. During free exploration sessions, rats were placed on the arena floor and recorded without any intervention except for infrequent behavioral checks or to adjust cables or connections. These non-rewarded sessions were run prior to the two rewarded sessions (as in Supp. Figs. 1 & 2) while the environment remained novel and prior to developing expectations of reward in the arena context. Note, one session for one rat was excluded because of data file corruption.

Behavioral comparisons.

Given the differences in the number and type of behavioral sessions between probe- and wire-implanted rats (Supp. Figs. 1 & 2), we compared behavioral measures between rewarded and non-rewarded sessions in two ways: Unpaired comparisons of behavioral measures were made using all sessions for all rats (df = 41) without correcting for unequal sampling to maximize the sample size. Paired comparisons (repeated-measures, df = 7) were made for probe-implanted rats using the last two unrewarded sessions and the two subsequent rewarded sessions to control for idiosyncratic tendencies (e.g. to explore or cower), thus better isolating the effect of session type. Unpaired comparisons in which the number of *rewarded* sessions was limited to two per rat showed the same pattern of results, but are not reported here for simplicity.

Derivation of delta, theta, and gamma amplitude timeseries.

To evaluate the correspondence of LFP dynamics in the delta-, theta-, and slow and fast gamma-frequency bands (1-4 Hz, 6-10 Hz, 25-55 Hz, and 65-120 Hz, respectively) to animals' movement speeds, we first derived amplitude timeseries for each frequency band for each recording site, as follows: Peaks and troughs of each band-pass filtered LFP signal were identified; half-cycle amplitudes were calculated directly by subtracting each trough from the adjacent peaks; and these amplitude values, assigned to the median timepoints of the corresponding trough-peak intervals, were then resampled to 2 kHz to give timeseries paralleling the original LFP recordings.

Movement speed modulation of HC rhythms.

Timeseries for movement speed and the amplitudes of each frequency band were mean-filtered with a two second sliding window using a one second step size. The two second window duration was chosen as a compromise between the relatively fast timescale of rats' locomotor behaviors, e.g. bouts of running and interspersed pauses, and the reduction in number of oscillatory cycles (particularly for delta) contributing to amplitude measures for shorter time windows. We then regressed movement speed onto the four frequency bands of interest for each HC recording site from rewarded behavioral sessions chosen for each rat (n=164). We compiled across all regression models the distributions of beta values for each frequency band that was a significant predictor of movement speed ($p<0.001$). We also generated the distributions of pairwise correlation coefficients between each frequency band and movement speed, as well as between pairs of frequency bands.

Spectral content and coherence of HC LFPs.

The power spectral density (PSD) of HC recordings was estimated using Welch's method for 2.05 second windows throughout each recording session. Raw PSDs were clustered hierarchically using MATLAB’s 'linkage' function into 16 groups based on frequency content below 25 Hz. This clustering approach was strongly influenced by PSD amplitude. We also clustered area-normalized versions of the same PSDs resulting in groupings emphasizing similarity of PSD waveforms independent of amplitude. In both cases, once cluster membership was determined, measures of delta and theta power were derived from the raw PSDs. Coherence estimates between each of six pairs of four simultaneously-recorded HC sites were obtained using MATLAB’s 'mscohere' function. The medians of these coherence estimates, derived for LFP timeseries for each instance of putative modes and behavioral bouts described above, were used for comparisons across conditions.

Histology.

After completion of all experiments, rats were anesthetized with isoflurane (5%) mixed with oxygen (800 ml/min) and marking lesions were made with a NanoZ (Plexon) to deliver 10μA for 10s at each of the 32 electrode locations. About an hour later, rats were transcardially perfused with 100 ml phosphate-buffered saline (PBS), followed by 200 ml of 4% paraformaldehyde (PFA, pH 7.4; Sigma-Aldrich, St. Louis, MO). Brains were post-fixed overnight in 4% PFA and then placed in a 30% sucrose solution for cryoprotection. Frozen brains were cut on a Leica CM3050 S cryostat (40 μm; coronal) and Nissl-stained. Marking lesions were mapped onto plates of the Paxinos & Watson Atlas (2018).

Results

Focusing on delta and theta frequency bands, we investigated the spectral content of HC LFPs while rats freely navigated a large 'open field' arena (122 cm x 118 cm) in both non-rewarded and sporadically-rewarded (dropped Fruit Loops®) session types (Fig. 1A&B). Locomotor coverage of the arena exhibited by one rat during representative sessions of each type is depicted in Figure 1B.

Overall behavior.

During both non-rewarded and rewarded sessions, rats were more often stationary (~20-40% and ~15-30% of session time, respectively) than walking or running at any other particular speed (Fig. 1C). As has been previously observed, a consistent peak in speed occupancy was evident at ~7 cm/s (e.g., Wirtshafter & Wilson, 2019) reflecting the prevalence of slower exploratory behaviors. Across all sessions the average distance traveled was 34.33 ± 13.71 m, with more distance covered in rewarded sessions (38.24 ± 15.76 m) than non-rewarded sessions (29.38 ± 8.67m; $t_{(41)} = 2.20$; P = 0.034). The corresponding average body movement speed across all sessions was 12.4 ± 4.8 cm/s, with faster movements during rewarded sessions (13.7 ± 5.8 cm/s) than non-rewarded sessions (10.6 ± 2.5 cm/s; $t_{(41)} = 2.18$; P = 0.035). A repeated measures comparison of average speed during consecutive non-rewarded (10.8 ± 3.1 cm/s) and rewarded session pairs (17.0 ± 8.5 cm/s) also indicated faster body movements (and reduced time spent stationary) during rewarded than non-rewarded sessions ($t_{(7)} = 2.7$, P = 0.030).

As is typical in open field experiments, rats tended to stay close to walls and corners of the arena (i.e., thigmotaxis, as in Fig. 1B, top) with an average across all sessions of 78.4 ± 18.7% time spent in the areas nearer to a wall and 21.6 ± 18.7% time in an equivalent central area. Reflecting arena-crossing routes taken while foraging, rats spent more time in the central space during rewarded sessions (29.5 ± 19.3%) compared to non-rewarded sessions (11.6 ± 12.2%; $t_{(41)} = 3.52$; P=0.0011), and this effect was robust to a repeated-measures comparison restricted to probe-implanted rats ($t_{(7)} = 2.82$; P=0.026). Figure 1B illustrates a striking example of the reduction in thigmotaxis (and the increase in distance traveled) that one rat exhibited during a rewarded session (bottom) relative to an unrewarded session (top).

Incidence of precisely-defined behavioral bouts.

In addition to spatial occupancy and movement speeds measured from body tracking data, we derived animals' body orientation, head angle, and rotational velocity by integrating tracking data for head-mounted LEDs with body tracking data (Fig. 1A). We found that rats' head angle exceeded 35 degrees (as when looking to the side or turning) during 15.3 ± 6.1% of each session, and rats' rotational velocity exceeded 52.5 degrees/sec during 14.1 ± 6.3% of each session. These proportions did not differ between session types (p = 0.39 and 0.59, respectively). Using these thresholds in conjunction with movement speed and duration criteria, we were able to precisely identify bouts of locomotor and stationary behavior, while excluding the majority of other fast movements (e.g., grooming) or movements *'in place'* (e.g., rearing).

The number of locomotor bouts exhibited per session varied widely between rats as well as across sessions (>2 sec duration: 5 to 63 bouts, mean = 21.3; >1 sec duration: 15 to 262 bouts, mean = 105.1), but neither the incidence nor the maximum duration of locomotor bouts (4.3 ± 1.0 sec and 4.1 ± 0.8 sec for rewarded and non-rewarded sessions, respectively) differed between session types using pairs of repeated measures ($P_{(2sec)}$=0.53 and $P_{(1sec)}$=0.27; $P_{(max)}$=0.82). However, average movement speeds during both two second and one second running bouts were modestly faster in rewarded sessions (29.2 ± 7.9 cm/sec)

than nonrewarded sessions (25.6 ± 5.9 cm/sec, $t_{(7)}$=2.57; P=0.037; $t_{(7)}$ = 2.77; P=0.028, respectively).

Behavioral trends across sessions.

The four probe-implanted rats did not exhibit any consistent relationship between behavioral measures and session number across the five *non-rewarded* sessions (Supp. Fig. 1 A-C, black traces). The coefficient of variation of activity level across rats (c.v. = 0.17, unitless) was twice the mean coefficient of variation across sessions for each rat (c.v. = 0.09). Similarly, coefficients of variation across rats were also greater than twice the within-rat coefficients for movement speed (0.24 > 0.12) and thigmotaxis (0.14 > 0.05). Thus, in the absence of rewards (and without any imposed task), rats' behavioral profiles were stable across sessions but quantitatively idiosyncratic (to each rat) in terms of activity levels, movement speeds, and thigmotaxis.

In contrast to the behavioral stability observed across *non-rewarded* sessions, the two wire-implanted rats exhibited trends across the eight *rewarded* sessions for reduced activity levels, movement speeds, and thigmotaxis in the later sessions (Supp. Fig. 1 D-F). The reductions in activity level and movement speed across sessions, potentially reflecting some combination of increased foraging efficiency, reduced anxiety, and reduced environmental novelty, amplify the observations that those measures were elevated in rewarded sessions relative to non-rewarded sessions conducted previously. Evaluation of bout-wise running behavior (Supp. Fig. 2) showed diminished or no such trends across successive sessions and session types. Interestingly, there was no apparent difference in the number of running bouts between early and late sessions or between session types (Supp. Fig. 2A). Taken together, our behavioral analyses suggest idiosyncrasies in rats' propensity to explore, but consistency across the temporal features of locomotor bouts and relationships to reward.

Recording sites in HC and mPFC.

HC electrodes were targeted to the proximal CA1-CA2 juncture (Fig. 2A & Fig. 2B, top panel) of the right dorsal HC (A/P: −2.52-3.72 mm, M/L: 1.00-3.00 mm). The majority of HC marking lesions were found in stratum lacunosum moleculare or stratum radiatum (M/L: 1.00-3.00 mm). Recordings from electrodes in the corpus callosum or CA3 were not analyzed. Marking lesions at recording sites distributed along the rostrocaudal extent of mPFC (Fig. 2B, bottom panel) were found primarily in the deep layers of anterior cingulate cortex and dorsal prelimbic cortex (A/P: 4.68-2.16 mm, M/L: 0.8-1.4 mm). In one rat, the lateral row of mPFC electrodes invaded motor cortex and those sites were excluded from further analysis (the medial row was on target and included).

Spectral content of HC LFPs during navigation.

The power and peak frequency of the HC theta rhythm (6-10 Hz), as well as theta-gamma cross-frequency coupling, have been shown to covary with an animal's running speed in several behavioral paradigms (Maurer et al., 2005, Hinman et al., 2016, Richard et al., 2013, Sheremet et al., 2019), and the theta rhythm is an important mechanistic component of episodic memory and spatial navigation models (Hasselmo, 2011, Buzsaki & Moser, 2013, Schultheiss et al., 2015). As expected, our HC LFP recordings consistently showed a

prominent theta rhythm as rats navigated the open field (Fig. 3A-C), and theta power was markedly elevated during faster locomotion (Fig. 3D-I). Spectrograms shown in Figure 3 (D, F, & H) illustrate the time-varying spectral content of HC LFPs and highlight the correspondence of theta power (warmer colors) to faster movements (peaks in white traces). Moreover, theta harmonic power (~16 Hz) often appeared in spectrograms coincident with peaks in movement speed (open stars). In striking contrast, significant power in the delta frequency band (1-4 Hz) often developed immediately when animals became still after periods of movement (e.g., filled stars in Fig. 3; Supp. Fig. 3). These delta events appeared in the spectrogram as tails descending from the theta band in tandem with pauses in rats' locomotor activity (white traces). Although elevated delta power typically persisted while animals remained stationary, LFP voltage traces generally did not show a stable, rhythmic delta oscillation with continuous phase progression across successive cycles. See Supp. Fig. 1A and Fig. 3A&B showing slow voltage fluctuations without well-organized periodicity.

Delta-band synchronization typically appeared in the power spectral density (PSD) for a given session as either a small distinct peak or as an asymmetric shoulder to the theta peak (Fig. 3 E, G, & I, top panels). These PSDs are equivalent to integrating the entire spectrogram over time into a single spectrum. In contrast, PSDs for shorter epochs (≤36 seconds) often showed either a sharply-tuned theta peak and very little delta power when animals were running fast, or elevated delta power without a prominent theta peak when animals were stationary (Fig. 3 E, G, & I, bottom panels). This observation led us to ask whether delta-band synchronization is (1) related to locomotor behavior, and (2) coupled to rhythmic activity in other frequency bands.

Correlations of 'rhythms' to movement speed.

To evaluate the hypothesis that HC delta synchrony (in addition to theta and gamma rhythms) is modulated by movement speed, we derived an instantaneous-amplitude timeseries for each frequency band for each LFP channel (Fig. 4A). The derivation of these timeseries used interpolation between the times of peak-to-trough measurements for each cycle at each frequency, yielding smoothly varying amplitude estimates with a constant sampling timestep. We then calculated the pairwise correlation coefficients between movement speed and the amplitude of each band (Fig. 4B) during a rewarded session for each rat, and we asked whether the distributions of r-values (across all recording sites in all rats) were different than zero. Conceptualized in this way, we found that delta, theta, and fast gamma were all related to movement speed (Fig. 4C). Theta and fast gamma amplitudes both covaried positively with movement speed, but strikingly, delta showed the strongest relationship to movement speed ($p=8.97x10^{-65}$) with negative r-values for >97% of HC recording sites (top left). Thus, whereas the theta and high gamma rhythms were strongest during fast running, delta power was strongest when animals were stationary or moving slowly and was diminished or absent during running. Moreover, using a four-predictor regression of movement speed onto delta, theta, and slow and fast gamma amplitudes, we found a significantly negative relationship of delta amplitude to speed and significantly positive relationships of theta and fast gamma to speed (Fig. 4D). Interestingly, many fewer recording sites exhibited speed modulation of slow gamma than of the other rhythms in the multiple regression (Fig. 4D), revealing a negative relationship to movement speed that was

not statistically detected using all pairwise correlations (Fig. 4C, top right). This pattern of relationships of the delta, theta, and gamma frequency bands to movement speed suggested the possibility of behavior-related interactions between bands (Sheremet et al., 2019).

Correlations between rhythms.

To assess amplitude-amplitude cross-frequency coupling between rhythms, we inspected the distributions across recording sites of correlation coefficients between each pair of frequency bands (Fig. 5). We found that (1) overall, delta and theta amplitudes exhibited a weak tendency toward negative covariation based on the distribution of r-values; (2) delta and fast gamma showed a bimodal distribution of r-values consisting of a prominent negative peak and a secondary peak centered near zero (indicated with arrowheads); and, (3) theta and fast gamma also showed a bimodal distribution of r-values, but both peaks occurred at distinctly positive values suggesting the possibility that different theta-fast gamma coupling modes (strengths) were expressed at different subsets of recording sites. To unpack the composition of these r-value distributions, we also inspected the relationships between frequency bands for each recording site independently. Scatter plots of amplitude measurements for each pair of bands revealed a diversity of complex relationships (Fig. 5, all insets). Representative examples from two rats shown in Figure 5 illustrate that delta and theta amplitudes could be either (1) orthogonal, such that larger values and the preponderance of variance in each band occurred at the smallest amplitudes of the other (A, top inset), or (2) weakly anticorrelated (A, bottom inset). Coalescence of these different delta-theta relationships is consistent with the modest negative peak in the r-value distribution. Scatterplots of delta and high gamma amplitudes showed similar relationships (B, insets), whereas theta and high gamma were positively correlated in most cases (C, insets). Importantly, these plots illustrate that correlated cross-frequency relationships are heterogenous across rats and recording sites, and each may comprise one or more distinct functional modes of cross-frequency coupling (suggested by dashed ellipses). Stationary behavior and running (color code for movement speed in all insets) consistently corresponded to different regions within 2-D cross-frequency amplitude spaces (insets), and amplitude relationships between bands exhibited characteristic slopes for each putative mode (i.e. the slope of the major axis of each ellipse, as in C, top inset).

Taken together, our analyses of speed modulation of HC LFP bands implicate the delta frequency band as a potentially important complement to theta and fast gamma rhythms in neural algorithms for navigation behavior. We focused subsequent analyses in the present report on delta and theta frequency bands, but it will be of considerable importance for further investigations to employ complementary approaches for estimating slow and fast gamma power (Zhou et al., 2019) in order to evaluate gamma relationships to behavior (Ahmed & Mehta, 2012, Zheng et al., 2015), hippocampal spiking (Zheng et al., 2016), and parahippocampal circuit dynamics (Colgin et al., 2009). Significant further investigation is also needed to identify and characterize possible contributions of HC delta synchrony to (1) neural representations of space or events during navigation, (2) resetting or refreshing network activity to maintain encoding fidelity, (3) retrieval of remembered information to plan or guide navigation of previously experienced contexts, or (4) encoding of spatial and behavioral trajectories into episodic memory. A key first step is to clarify whether instances

of strong delta synchrony and instances of strong theta synchrony represent distinct functional modes of network activity that are mutually-exclusive, or whether the two frequency bands can vary smoothly in opposition to one another, one waxing as the other wanes.

Clustering approach to classification of spectral modes.

Given the considerable behavioral variability between rats in our experiments and the dependence of delta- and theta-frequency synchrony on navigation behaviors, we devised a simple, behaviorally-robust analytic strategy to categorize putative modes of HC network activity based on the power spectral density (PSD) of the LFP (Fig. 6A-C). Briefly, we applied hierarchical clustering routines to the power spectra (0.7-25 Hz) for two second windows of the HC LFP throughout each behavioral session (i.e., the spectrogram). This general strategy for unsupervised categorization of network modes can be implemented in numerous ways using different clustering algorithms and parameter settings to focus on different aspects of the relationships between animals' behavior and LFP spectra. We chose parameters to balance the frequency resolution of PSDs with the ability to analyze tracking data at behavioral timescales.

Figure 6A shows ~4000 superimposed time-windowed PSDs (for timepoints throughout behavioral sessions) for two representative LFP channels from each of three rats. 'Spectral modes' derived by clustering windowed PSDs and defined as the average PSD for each cluster (Fig. 6B) were used to operationalize putative functional modes of HC network activity. Each spectral mode corresponded to a vector of times at which the LFP showed a particular pattern of spectral content. That is, applying clustering routines to the spectrogram generated a timeline of the incidence of each spectral mode, which in turn enabled evaluation of whether specific aspects of neural activity (e.g. power in a specific band) or of behavior (e.g. running speed) varied between the sets of times when different modes occurred.

Delta-theta orthogonality.

We found that delta power and theta power were strikingly orthogonal across spectral modes (Fig. 6B-D). This orthogonal relationship was consistently pronounced across rats and recording sites, amplifying our previous demonstration that strong delta or theta typically occurred when synchrony in the other band was weak. Figure 6B shows the spectral modes derived from the windowed PSD 'stacks' in Figure 6A, sorted loosely according to peak frequency. Spectral modes almost always consisted of a single primary peak occurring at a frequency within the delta band or within the theta band, but not between delta and theta, particularly if the peak was of substantial amplitude (Fig. 6B). We also applied our clustering routines to stacks of area-normalized (<25 Hz) windowed PSDs. This manner of classifying spectral modes emphasized the relative power between frequency bands allowing the waveform of lower amplitude PSDs to contribute to mode classifications. With this more-conservative approach, we found a similar selectivity of spectral modes for either delta or theta (Fig. 6C). Note the consistent absence of modes with peaks between the delta and theta bands, as well as the absence or diminutiveness of secondary peaks for individual modes (Fig. 6C, green or blue traces). Figure 6D illustrates delta-theta orthogonality as the

'elbow' in plots of the relative power for the two bands across modes. Taken together these observations suggest that delta-theta orthogonality does not represent complete independence of the two frequency bands, but rather a *'permissive/exclusive'* relationship. That is, if delta and theta are directly mechanistically coupled in some way, delta-theta orthogonality can be framed either as mutual-exclusivity between strong delta synchrony and strong theta synchrony, or as permissiveness of elevated synchrony in one frequency band by minimization of synchrony in the other. In this case, the mechanism of switching between modes is a fundamental question in complement to mechanisms underlying delta function. Alternatively, delta-theta orthogonality could reflect couplings to different aspects of behavior or other third variables.

Temporal alternation of delta and theta modes.

Delta and theta amplitude timeseries (as in Fig. 6E) showed that transitions between delta and theta often occurred rapidly, within a few seconds (as in Supp. Fig. 3), indicating that delta and theta modes could alternate during behavior sufficiently fast to implement different aspects of spatial encoding, decision, or memory processes. Fast 'state-like' transitions, whereby synchrony in one frequency band was replaced suddenly by synchrony in the other band were common (Fig. 6E, filled stars); but interestingly, these transitions were not always clean. In some instances, delta and theta fluctuated together (correlated positively) at a fast timescale, despite ongoing divergence between the two at longer timescales (Fig. 6E, open stars). Such 'multi-scale transitions' could be spurious or may represent nested neurophysiological phenomena of particular consequence. It will be important to determine what the impact of brief bouts or prolonged epochs of correlated delta and theta would be for encoding and plasticity in HC networks.

Correspondence of modes to behavior.

To begin to ask whether spectral modes are functionally distinct, we first evaluated whether animals' behavior differed between times at which different modes occurred. We found that average delta power across spectral modes (classified using either unnormalized or normalized PSDs) was orthogonal to animals' movement speeds (Fig. 7A&B, left panels). Contrastingly, theta power across spectral modes was strikingly correlated to movement speed, and this relationship was consistent across all rats and recordings sites (n=24, i.e. 4 channels per each of 6 rats; $t_{(23)}=5.16$; $P=3.14\text{x}10^{-5}$, Fig. 7A&B, right panels). Next, we evaluated intra-HC phase coherence (between pairs of recording sites) as a function of spectral modes. Figure 7C shows the coherence spectra for each mode from a representative session. Note that coherence spectra with high delta-band coherence exhibited the least theta-band coherence (blue traces), and spectra showing high theta coherence had weak delta coherence (green traces). Lastly, using the ratio of theta power to delta power (TDR), a common neuropsychiatric diagnostic tool, we found that intrahippocampal delta coherence across modes consistently declined with increasing TDR ($t_{(23)}=-5.97$; $P=4.35\text{x}10^{-6}$). In contrast, theta coherence increased with increasing TDR ($t_{(23)}=4.912$; $P=5.8\text{x}10^{-5}$, Fig. 7D, Supp. Fig. 4) which in turn tracked animals' movement speeds.

We have shown that across an entire recording session the amplitude of delta, theta, and gamma frequency bands are all related to movement speed, and band-pass amplitudes are

coupled in a speed-dependent manner. We have also shown that classification of HC network modes, purely by clustering power spectra, yields groupings that correlate with movement speed and intrahippocampal coherence, indicating that these modes are functionally distinguishable.

Delta-theta dynamics during bouts of running and stationary behaviors.

In a last series of analyses, we integrated tracking data for rats' head-mounted LEDs with body-tracking data to derive measures of animals' head angle (relative to the body) and rotational velocity (Fig. 8A, top). We then used these measures to isolate bouts of running and stationary behavior, while excluding grooming, rearing, and other behaviors that incorporate fast turning or angled body postures. Figure 8A illustrates how these exclusions (red circles) were made. The resultant precisely-defined behavioral bouts occurred throughout the open field environment (Fig. 8B) without notable biases that weren't evident in the full sets of tracking data (other than thigmotaxis, for example). As described earlier, our analyses showed qualitative similarity between rats' behavior (Fig. 8C) despite moderate idiosyncrasies in rats' propensities to initiate running bouts at different speeds or to halt and remain sufficiently stationary to meet our bout criteria (Fig. 8D&E). We found that delta power in HC was elevated when rats paused between runs even briefly, and elevated theta power tracked average and peak speeds during running bouts. Behavior and LFP spectral content for typical bouts of intermittent running and interspersed stationary bouts are shown in Figure 8 (D, F, and G); and bout-wise relationships between delta, theta, and running speed replicated cleanly our earlier demonstrations of delta-theta orthogonality (Fig. 8H).

Lastly, we focused on the two rats implanted for dual-site recordings from HC and mPFC to evaluate whether delta- and theta-dominated HC modes represent components of larger-scale distributed-circuit function during different behaviors. We evaluated delta-band and theta-band mPFC-HC coherence between running and stationary bouts collected across the eight rewarded behavioral sessions for each animal (907 total two second bouts and 3649 one second bouts). With no assumption of equal variances in the distributions of coherence values between bout types, we found that delta coherence between mPFC and HC was elevated during stationary bouts that were at least two seconds in duration ($t_{(905)}=4.34$; $P=1.61\text{x}10^{-5}$), and theta coherence was elevated during running bouts ($t_{(905)}=-13.21$; $P=1.40\text{x}10^{-36}$). Using a one second minimum bout duration allowed inclusion of bouts nested within more heterogenous behavioral episodes, because animals weren't required to maintain a given behavior for as long. Still, delta-band mPFC-HC coherence was increased robustly when animals were stationary ($t_{(3637)}=6.77$; $P=1.50\text{x}10^{-11}$), and theta coherence was increased during running ($t_{(3637)}=-18.64$; $P=3.88\text{x}10^{-74}$). Thus, even at fast behavioral timescales, spectral modes of HC network activity may be considered to be components of larger-scale patterns of functional activity across brain regions (distributed-circuit modes) that likely reflect the semi-modular neural implementation of complex cognitive processes for navigation and episodic encoding.

Discussion

We evaluated awake delta and theta rhythms in hippocampal LFP recordings for relationships to behavior, to each other, and to network coordination, using measures of the instantaneous amplitude in each frequency band, short time-windowed power spectral densities (PSDs), and coherence. We identified *spectral modes* of HC activity using a novel analytic approach in which we applied hierarchical clustering to the time-windowed PSDs that comprise the spectrogram. We found that delta- and theta-frequency synchronization were orthogonal across spectral modes suggesting a qualitative difference in network states, rather than an anticorrelation between two continuously varying network properties. Independent of clustering parameters and session type, delta- and theta-modes mapped closely onto animals' locomotor behaviors, as well as to intrahippocampal coherence, and paralleled differences in mPFC-HC coherences between precisely-defined behavioral bouts. Thus, we suggest that our operationally-defined data-driven *spectral modes* are representative of functional modes of hippocampal network activity, and that HC modes may be components of larger-scale circuit modes corresponding to distributed cognitive functions.

Awake delta.

Of particular note, we consistently observed *awake delta* in hippocampal spectrograms as rats freely navigated an open field. In contrast to the theta rhythm, delta appeared in tandem with pauses in rats' saltatory locomotor trajectories, i.e. interspersed between periods of theta-dominated HC activity during intermittent running. We confirmed that delta power was negatively related to locomotion with correlational analyses of 164 recording sites (across six animals) near the junction of proximal CA1 and CA2 in dorsal HC. The overwhelming consistency of this relationship was surprising given the relative scarcity of reports characterizing delta-frequency activity in awake animals. We suspect awake delta has been overlooked to some extent, at least in hippocampus, because of methodological considerations related to investigative focus on the theta rhythm. For example, delta can be excluded by low-cut filtering the LFP or by restricting data analyses using a minimum-threshold criterion for the theta-delta ratio, either to identify epochs of strong theta activity or to avoid potentially interpreting recording instability as neural activity. Furthermore, studies of hippocampal function generally focus on periods when animals are moving or are otherwise actively engaged in task-related behaviors, times when delta would be absent. Lastly, awake delta may be deemphasized in analyses of hippocampal and cortical recordings, because of an implicit assumption that it would be mechanistically related to delta waves seen in slow wave sleep. Since delta waves during sleep have been considered periods of cortical silence, awake delta would then seem to offer little depth to be explored. However, any relationships of awake delta to delta waves during sleep remain to be characterized. Given the recent demonstration of memory-related delta spikes during sleep (Todorova et al., 2019), awake delta may in fact be of particular importance to episodic encoding, *especially* if it bears mechanistic commonalities to delta during sleep.

Task-independence of delta and theta relationships to behavior.

Despite the relative lack of attention that delta synchronization in HC has received, we found that awake delta was prominent and delta-theta orthogonality was consistently apparent during both non-rewarded and rewarded session types. This robustness suggests a potentially fundamental role of delta modes, in contrast or in complement to theta modes, during navigation in behavioral contexts that would be expected to differ in terms of animals' motivational states (for rewards) and attentional or other cognitive states visited during foraging. Because both delta and theta synchrony are related to behavior, differences in behavior between session types would also be expected to impact the appearance of delta and theta modes. In fact, delta modes tended to be more consistent in non-rewarded sessions in which animals were more sedentary, and theta modes tended to be most prevalent in sessions where animals consistently foraged for rewards throughout the arena.

The consistency of awake delta's relationship to locomotor behavior was also surprising given differences in synaptic input and local circuitry across regions and cortical layers sampled by our recordings. Although not specifically addressed by our current analyses, it is a strong hypothesis that there is an anatomical layout in HC wherein delta is stronger in some regions and theta in others, reflecting synaptic inputs to particular regions within the laminar structure of HC or along the proximal-distal or septo-temporal axes. Our preliminary analysis of cross-frequency couplings indicated the possibility that delta-theta, delta-gamma, and theta-gamma relationships may also reflect the anatomical distribution of recording sites as well as behavioral state. Such a mapping would be expected to relate to coherence measures between sites within HC and with other structures. To the extent that we evaluated intrahippocampal and mPFC-HC coherence, we found that coherence spectra for pairs of recording sites tended to fall into fairly homogenous groupings of similar coherence spectra that were often markedly distinct from one another (coherence clusters, not detailed here). We suspect that these groupings delineate important anatomical boundaries, possibly related to limbic thalamic circuitry (Dolleman van der Weel et al., 2019). Application of data-driven clustering routines to coherence spectra is likely to be a fruitful approach for further defining network and circuit modes in this (or any) system, as will be analytic integrations of independent mode definitions including clusters derived from different recording sites and clusters derived using frequency decomposition methods and classifiers better suited to distinguishing features of gamma rhythms in different sub-bands.

LFP spectral modes as representative of functional neural modes.

We conceptualize *functional modes* of neural computation as input-output (I-O) functions implemented at any scale of neural machinery by neurons, local networks, or distributed circuits. By this formulation, the role of *network* modes occupies the computational space (non-inclusively) between information encoding by ensembles of specific neurons at behavioral timescales, i.e. specific representations, and more global brain states driven by wakefulness or sleep, behavioral engagement, anesthetic influence, seizure, etc. Because the LFP reflects synchrony among synaptic potentials from local network interactions and long-range inputs, we reasoned that (1) the computational states of the neural tissue surrounding our recording electrodes should be consistent in terms of the I-O transforms being applied to inputs and the corresponding patterns of synchrony, and (2) those patterns of synchrony may

be distinguishable by the spectral content of the LFP. If so, classification of short time-windowed power spectra should distinguish functional modes of the local network in such a manner that, for example, network representations of different environments (specific maps or attractors) or locations within an environment would be expected to group together in a common mode, whereas distinct cognitive states or processes that fluctuate at behavioral timescales (or more slowly) should be classified differently. Our clustering approach to identifying *spectral modes* implemented this reasoning while remaining agnostic to potential profiles of LFP spectral content across well-characterized (or neglected) frequency bands.

Whereas modes with strong theta power typically had minimal power in the delta band, we observed that modes with elevated delta power tended to exhibit minimal power in the theta band. Therefore, we interpret the orthogonality of delta power and theta power as potentially reflective of a permissive/exclusive relationship between two categories of functional neural modes. It is important to note that, although spectral modes tended to exhibit peaks in the PSD that were segregated to either the delta band or to the theta band, individual modes exhibited peaks at a wide range of frequencies within the respective bands. The magnitudes of delta and theta peaks in the PSD also varied widely across spectral modes.

Our analyses do not address potential commonalities between delta- or theta-dominated modes in our data and respiration-related rhythms that have been seen in widespread brain regions (Tort et al., 2018) or the 4 Hz oscillation identified by Fujisawa and Buzsáki (2011) to mediate functional coupling within circuits including hippocampus during working memory tasks. Functionally-distinct rhythms can operate in overlapping frequency bands (simultaneously or not). Our analytic strategy could be extended in the future to dissociate rhythms using clustering routines that precisely target dimensions (and ranges) by which the rhythms are distinguishable, either in the fine structure of LFP spectra, cycle-by-cycle measures of raw or filtered LFP traces, or fast time-scale interactions between frequency bands or recording sites. Additional insight will be gained by applying the clustering approach to multiple simultaneous recordings, either by some integration of spectral modes from multiple LFP sources (between or within brain areas), or by classifying momentary short-time coherence spectra (between patterns of channels) throughout behavioral sessions.

From the present data set it is not possible to determine what cognitive, behavioral, or physiological dimensions might be encoded by the two-to-five-fold differences in delta power that were typical in our experiments, nor by the distribution of power across the delta frequency range (including one or more peaks). On the one hand, one might assume that the degree of synchronization and temporal dynamics of delta-frequency activity are purely epiphenomenal to the integration of up-/down-state transitions from many semi-independent columns across widespread cortical regions that project to the HC. However, it is worth noting that delta-dominated network modes that materialize rapidly, and that punctuate animals' behavioral and cognitive state trajectories, are incredibly well-positioned to influence memory-guided decision making and behavior, or to implement the first steps of episodic memory encoding. Thus, fast timescale metrics of delta should be evaluated for behavioral and neurophysiological correlates. To contextualize the role of awake delta for episodic memory and other cognitive functions it will be important to consider if and how awake delta in proximal CA1/CA2 may be related to mechanisms of spatial coding

(Henriksen et al., 2010, Igarashi et al., 2014), initiation of sharp-wave ripples in CA2 and ripple-related coordination of HC interactions with mPFC and reward structures (Oliva et al., 2016, Jadhav et al., 2016, Sosa et al., 2020), and neurophysiological dysfunctions including working memory deficits in disease states, e.g. schizophrenia (Duan et al., 2015) and epilepsy (Chevaleyre and Piskorowski, 2016). The appearance of delta modes at pauses in locomotor behavior could also reflect the phase-resetting of oscillatory mechanisms for navigation that otherwise might accumulate error over longer distances or durations of uninterrupted running. Similarly, delta modes could reset activity patterns within functional networks (e.g. of head direction or grid cells in parahippocampal regions) to maintain calibration of representations of orientation or spatial scale.

A critical question raised by the present work is whether awake delta is a mode or the absence of a mode. Although, the independence of or interdependencies between mechanisms underlying delta, theta, and gamma synchronization remain to be elaborated, some context may be gained by extrapolation from what is known (or believed) about the theta rhythm. Individual theta cycles can be considered independent computational units (e.g. Mizuseki et al., 2009, Eliav et al., 2018) with specific gamma profiles (e.g. Amemiya et al., 2018, Lopes-Dos-Santos 2018). If future inquiries into awake delta should demonstrate functionally-relevant ensemble activity or cross-frequency coupling, i.e., if delta proves to be a functional mode of neural computation, the timing of delta beats (Supp. Fig. 3) within behavioral (and cognitive) trajectories and relative to theta-modes suggests it could be critical for segmentation of sequences of events in neural representations or ongoing or remembered episodes.

Notably, Hasselmo and colleagues (2002) suggested that encoding and retrieval mechanisms for episodic memory may be preferentially engaged at different phases of the theta rhythm when different inputs to CA1 are active (Schomburg et al., 2014). One provocative interpretation of alternating delta and theta modes during behavior is similar to observations of alternating theta-cycle-linked representations (Kay et al., 2020) and distinct theta-phase-linked mnemonic functions, albeit operating at a slower timescale. It could be imagined that these or other mnemonic or cognitive functions are preferentially engaged by alternating locomotor and stationary segments of behavioral sequences and corresponding theta- and delta-dominated circuit dynamics. In such a general formulation, awake delta-dominated states could be taken to reflect some form of meditation on or digestion of recent and ongoing experiences (similar to Todorova and Zugaro, 2019), or retrieval events for decision making and planning of upcoming actions.

Behaviorally, locomotor pauses segment sequences of actions or events within an episodic organization. Likewise, could awake delta-dominated modes mechanistically contribute to the segmentation of episodic memories? Further study will be necessary to determine what neural mechanisms underlie awake delta in HC and mPFC, as well as what mechanisms may elicit switching in either direction between delta and theta modes with changes in behavior. Is there a predominance of cortical silence during awake delta modes as had been previously been ascribed to delta waves during slow wave sleep? Or do prospective or retrospective representations exist during awake delta modes that could be of particular importance for encoding aspects of ongoing experience to guide future behavior? Inquiry into these and

other important questions motivated by the present work should greatly improve our understanding of what exactly we're doing when we stop to think.

Supplementary Material

Refer to Web version on PubMed Central for supplementary material.

Acknowledgements:

This work was supported, in part, by R01 ES006189 to T.R.G., R01 MH113626 to T.A.A. and funding from the Feinberg Foundation provided to T.A.A.

References

Ahmed OJ & Mehta MR (2012). Running speed alters the frequency of hippocampal gamma oscillations. Journal of Neuroscience, 32(21), 7373–7383. [PubMed: 22623683]

Amemiya S, & Redish AD (2018). Hippocampal theta-gamma coupling reflects state-dependent information processing in decision making. Cell Reports, 22(12), 3328–3338. [PubMed: 29562187]

Amzica F, & Steriade M (1998). Electrophysiological correlates of sleep delta waves1Correspondence and reprint requests may be addressed to either author.1. Electroencephalography and Clinical Neurophysiology, 107(2), 69–83. [PubMed: 9751278]

Barth AM, Domonkos A, Fernandez-Ruiz A, Freund TF, & Varga V (2018). Hippocampal network dynamics during rearing episodes. Cell Reports, 23(6), 1706–1715. [PubMed: 29742427]

Bennett C, Arroyo S, & Hestrin S (2013). Subthreshold Mechanisms Underlying State-Dependent Modulation of Visual Responses. Neuron, 80(2), 350–357. [PubMed: 24139040]

Bland BH, & Oddie SD (2001). Theta band oscillation and synchrony in the hippocampal formation and associated structures: the case for its role in sensorimotor integration. Behavioural Brain Research, 127(1), 119–136. [PubMed: 11718888]

Buzsáki G, (2002). Theta oscillations in the hippocampus, Neuron, 33(3), 325–340. [PubMed: 11832222]

Buzsáki G, & Moser EI (2013). Memory, navigation and theta rhythm in the hippocampal-entorhinal system. Nature Neuroscience, 16(2), 130–138. [PubMed: 23354386]

Canolty RT, Edwards E, Dalal SS, Soltani M, Nagarajan SS, Kirsch HE, … Knight RT (2006). High gamma power is phase-locked to theta oscillations in human neocortex. Science, 313(5793), 1626–1628. [PubMed: 16973878]

Chevaleyre V, & Piskorowski RA (2016) Hippocampal area CA2: An overlooked but promising therapeutic target. Trends in Molecular Medicine, 22(8), 645–655. [PubMed: 27372610]

Colgin LL, Denninger T, Fyhn M, Hafting T, Bonnevie T, Jensen O, Moser M, & Moser EI (2009). Frequency of gamma oscillations routes flow of information in the hippocampus. Nature, 462, 353–357. [PubMed: 19924214]

Colgin LL (2015). Do slow and fast gamma rhythms correspond to distinct functional states in the hippocampal network? Brain Research, 1621, 309–315. [PubMed: 25591484]

Dolleman-van der Weel MJ, Griffin AL, Ito HT, Shapiro MS, Witter MP, Vertes RP, & Allen TA (2019). The nucleus reuniens of the thalamus sits at the nexus of a hippocampus and medial prefrontal cortex circuit enabling memory and behavior. Learning & Memory, 26, 191–205. [PubMed: 31209114]

Duan H-F, Gan J-L, Yang J-M, Cheng Z-X, Gao C-Y, Shi Z-J, Zhu X-Q, Liang X-J, & Zhao L-M (2015). A longitudinal study on intrinsic connectivity of hippocampus associated with positive symptom in first-episode schizophrenia. Behavioural Brain Research, 283, 78–86. [PubMed: 25619684]

Eliav T, Maya G-S, Yartsev MM, Finkelstein A, Rubin A, Las L, & Ulanovsky N (2018). Nonoscillatory phase coding and synchronization in the bat hippocampal formation. Cell, 175(4), 1119–1130. [PubMed: 30318145]

Foster DJ, & Wilson MA (2007). Hippocampal theta sequences. Hippocampus, 17(11), 1093–1099. [PubMed: 17663452]

Fujisawa S & Buzsaki G (2011). A 4 Hz oscillation adaptively synchronizes prefrontal, VTA, and hippocampal activities. Neuron, 72(1), 153–165. [PubMed: 21982376]

Hasselmo ME, Bodelón C, & Wyble BP (2002). A proposed function for hippocampal theta rhythm: Separate phases of encoding and retrieval enhance reversal of prior learning. Neural Computation, 14(4), 793–817. [PubMed: 11936962]

Hasselmo ME (2012). How we remember: Brain mechanisms of episodic memory. MIT Press.

Henriksen EJ, Colgin LL, Barnes CA, Witter MP, Moser M-B, & Moser EI (2010). Spatial representation along the proximodistal axis of CA1. Neuron, 68(1), 127–137. [PubMed: 20920796]

Hinman JR, Brandon MP, Climer JR, Chapman GW, & Hasselmo ME (2016). Multiple running speed signals in medial entorhinal cortex. Neuron, 91(3), 666–679. [PubMed: 27427460]

Igarashi KM, Lu L, Colgin LL, Moser M, & Moser EI (2014). Coordination of entorhinal-hippocampal ensemble activity during associative learning. Nature, 510, 143–147. [PubMed: 24739966]

Jadhav SP, Rothschild G, Roumis DK, & Frank LM (2016). Coordinated excitation and inhibition of prefrontal ensembles during awake hippocampal sharp-wave ripple events. Neuron, 90(1), 113–127. [PubMed: 26971950]

Johnson A & Redish AD (2007). Neural ensembles CA3 transiently encode paths forward animal decision point. The Journal of Neuroscience, 27, 12176–12189. [PubMed: 17989284]

Kandel A, & Buzsáki G (1997). Cellular–synaptic generation of sleep spindles, spike-and-wave discharges, and evoked thalamocortical responses in the neocortex of the rat. The Journal of Neuroscience, 17(17), 6783. [PubMed: 9254689]

Kay K, Chung JE, Sosa M, Schor JS, Karlsson MP, Larkin MC, Liu DF, & Frank LM (2020). Constant sub-second cycling between representations of possible futures in the hippocampus. Cell, 180(3), 552–567. [PubMed: 32004462]

Lakatos P, Shah AS, Knuth KH, Ulbert I, Karmos G, & Schroeder CE (2005). An oscillatory hierarchy controlling neuronal excitability and stimulus processing in the auditory cortex. Journal of Neurophysiology, 94(3), 1904–1911. [PubMed: 15901760]

Lisman JE, & Jensen O (2013). The theta-gamma neural code. Neuron, 77, 1002–1016. [PubMed: 23522038]

Lopes-dos-Santos V, van der Ven GM, Morley A, Trouche S, Campo-Urriza N, Dupret D (2018). Parsing hippocampal theta oscillations by nested spectral components during spatial exploration and memory-guided behavior. Neuron, 100(4), 940–952. [PubMed: 30344040]

Maurer AP, VanRhoads SR, Sutherland GR, Lipa P, & McNaughton BL (2005). Self-motion and the origin of differential spatial scaling along the septo-temporal axis of the hippocampus. Hippocampus, 15(7), 841–852. [PubMed: 16145692]

McFarland WL, Teitelbaum H, & Hedges EK (1975). Relationship between hippocampal theta activity and running speed in the rat. Journal of Comparative and Physiological Psychology, 88(1), 324–328. [PubMed: 1120805]

Mizuseki K, Sirota A, Pastalkova E, & Buzsáki G (2009). Theta oscillations provide temporal windows for local circuit computation in the entorhinal-hippocampal loop. Neuron, 64(2), 267–280. [PubMed: 19874793]

Niell CM, & Stryker MP (2010). Modulation of visual responses by behavioral state in mouse visual cortex. Neuron, 65(4), 472–479. [PubMed: 20188652]

O'Keefe J & Recce ML (1993). Phase relationship between hippocampal place units and the EEG theta rhythm. Hippocampus, 3: 317–330. [PubMed: 8353611]

Oliva A, Fernández-Ruiz A, Buzsáki G, & Berényi A (2016) Role of hippocampal CA2 region in triggering sharp-wave ripples. Neuron, 91(6), 1342–1355. [PubMed: 27593179]

Pfeiffer BE, & Foster DJ (2013). Hippocampal place-cell sequences depict future paths to remembered goals. Nature, 497(7447), 74–79. [PubMed: 23594744]

Poulet JFA, & Petersen CCH (2008). Internal brain state regulates membrane potential synchrony in barrel cortex of behaving mice. Nature, 454(7206), 881–885. [PubMed: 18633351]

Redish AD (2016). Vicarious trial and error. Nature Reviews Neuroscience, 17(3), 147–159. [PubMed: 26891625]

Richard GR, Titiz A, Tyler A, Holmes GL, Scott RC, & Lenck-Santini P-P (2013). Speed modulation of hippocampal theta frequency correlates with spatial memory performance. Hippocampus, 23(12), 1269–1279. [PubMed: 23832676]

Sachdev RNS, Gaspard N, Gerrard JL, Hirsch LJ, Spencer DD, & Zaveri HP (2015). Delta rhythm in wakefulness: Evidence from intracranial recordings in human beings. Journal of Neurophysiology, 114(2), 1248–1254. [PubMed: 26084904]

Saleem AB, Ayaz A, Jeffery KJ, Harris KD, & Carandini M (2013). Integration of visual motion and locomotion in mouse visual cortex. Nature Neuroscience, 16(12), 1864–1869. [PubMed: 24185423]

Saleem AB, Ayaz A, Jeffery KJ, Harris KD, & Carandini M (2013). Integration of visual motion and locomotion in mouse visual cortex. Nature Neuroscience, 16(12), 1864–1869. [PubMed: 24185423]

Schacter DL, Addis DR & Buckner RL (2007). Remembering the past to imagine the future: the prospective brain. Nat. Rev. Neurosci 8, 657–661. [PubMed: 17700624]

Schultheiss NW, Hinman JR, & Hasselmo ME (2015). Models and Theoretical Frameworks for Hippocampal and Entorhinal Cortex Function in Memory and Navigation. In: Tatsuno M (eds) Analysis and Modeling of Coordinated Multi-neuronal Activity. Springer Series in Computational Neuroscience, vol 12. Springer, New York, NY

Schomburg EW, Fernández-Ruiz A, Mizuseki K, Berényi A, Anastassiou CA, Koch C, & Buzsáki G (2014). Theta phase segregation of input-specific gamma patterns in entorhinal-hippocampal networks. Neuron, 84(2), 470–485. [PubMed: 25263753]

Sheremet A, Kennedy JP, Qin Y, Zhou Y, Lovett SD, Burke SN, & Maurer AP (2019). Theta-gamma cascades and running speed. Journal of Neurophysiology, 121(2), 444–458. [PubMed: 30517044]

Shirvalkar PR, Rapp PR, & Shapiro ML (2010). Bidirectional changes to hippocampal theta-gamma comodulation predict memory for recent spatial episodes. Proceedings of the National Academy of Sciences USA, 107(15), 7054–7059.

Sirota A, & Buzsáki G (2005). Interaction between neocortical and hippocampal networks via slow oscillations. Thalamus & Related Systems, 3(4), 245–259. [PubMed: 18185848]

Sirota A, Montgomery S, Fujisawa S, Isomura Y, Zugaro M, & Buzsáki G (2008). Entrainment of neocortical neurons and gamma oscillations by the hippocampal theta rhythm. Neuron, 60(4), 683–697. [PubMed: 19038224]

Sosa M, Joo HR, & Frank LM (2020). Dorsal and ventral hippocampal sharp-wave ripples activate distinct nucleus accumbens networks. Neuron, 105(4), 725–741. [PubMed: 31864947]

Steriade M, Nunez A, & Amzica F (1993). A novel slow (<1 Hz) oscillation of neocortical neurons in vivo: depolarizing and hyperpolarizing components. The Journal of Neuroscience, 13(8), 3252. [PubMed: 8340806]

Tan AYY, Chen Y, Scholl B, Seidemann E, & Priebe NJ (2014). Sensory stimulation shifts visual cortex from synchronous to asynchronous states. Nature, 509(7499), 226–229. [PubMed: 24695217]

Todorova R, Zugaro M (2019) Isolated cortical computations during delta waves support memory consolidation. Science, 366:377–381. [PubMed: 31624215]

Tort ABL, Komorowski RW, Manns JR, Kopell NJ, & Eichenbaum H (2009). Theta–gamma coupling increases during the learning of item–context associations. In Proc Natl Acad Sci U S A (Vol. 106, pp. 20942–20947). [PubMed: 19934062]

Tort ABL, Brankack J, & Draguhn A (2018). Respiration-entrained brain rhythms are global but often overlooked. Trends in Neuroscience, 41(4), 186–197.

Van Der Meer MAA, & Redish AD (2011). Theta phase precession in rat ventral striatum links place and reward information. Journal of Neuroscience, 31(8), 2843–2854. [PubMed: 21414906]

van der Meer MAA, & Redish AD (2011). Theta phase precession in rat ventral striatum links place and reward information. The Journal of Neuroscience, 31(8), 2843. [PubMed: 21414906]

Vinck M, Batista-Brito R, Knoblich U, & Cardin JA (2015). Arousal and locomotion make distinct contributions to cortical activity patterns and visual encoding. Neuron, 86(3), 740–754. [PubMed: 25892300]

Vyazovskiy VV, Olcese U, Hanlon EC, Nir Y, Cirelli C, & Tononi G (2011). Local sleep in awake rats. Nature, 472(7344), 443–447. [PubMed: 21525926]

Vyazovskiy VV, Olcese U, Lazimy YM, Faraguna U, Esser SK, Williams JC, … Tononi G (2009). Cortical Firing and Sleep Homeostasis. Neuron, 63(6), 865–878. [PubMed: 19778514]

Whishaw IQ, & Vanderwolf CH (1973). Hippocampal EEG and behavior: Change in amplitude and frequency of RSA (Theta rhythm) associated with spontaneous and learned movement patterns in rats and cats. Behavioral Biology, 8(4), 461–484. [PubMed: 4350255]

Winson J (1978). Loss of hippocampal theta rhythm results in spatial memory deficit in the rat. Science, 201(4351), 160. [PubMed: 663646]

Wirtshafter HS, & Wilson MA (2019). Locomotor and hippocampal processing converge in the lateral septum. Current Biology, 29(19), 3177–3192.e3173. [PubMed: 31543450]

Zagha E, Casale Amanda E., Sachdev Robert N. S., McGinley Matthew J., & McCormick David A. (2013). Motor cortex feedback influences sensory processing by modulating network state. Neuron, 79(3), 567–578. [PubMed: 23850595]

Zhang L, Lee J, Rozell C, & Singer AC (2019). Sub-second dynamics of theta-gamma coupling in hippocampal CA1. eLife, 8.e:44320. [PubMed: 31355744]

Zheng C, Bieri KW, Trettel SG, Colgin LL (2015). The relationship between gamma frequency and running speed differs for slow and fast gamma rhythms in freely behaving rats. Hippocampus, 25(8), 924–938. [PubMed: 25601003]

Zheng C, Bieri KW, Hsiao Y, & Colgin LL (2016). Spatial sequence coding differs during slow and fast gamma rhythms in the hippocampus. Neuron, 89(2), 398–408. [PubMed: 26774162]

Zhou Y, Sheremet A, Qin Y, Kennedy JP, DiCola NM, Burke SN, Maurer AP (2019). Methodological considerations on the use of different spectral decomposition algorithms to study hippocampal rhythms. eNeuro, 6(4), ENEURO.0142-19.2019.

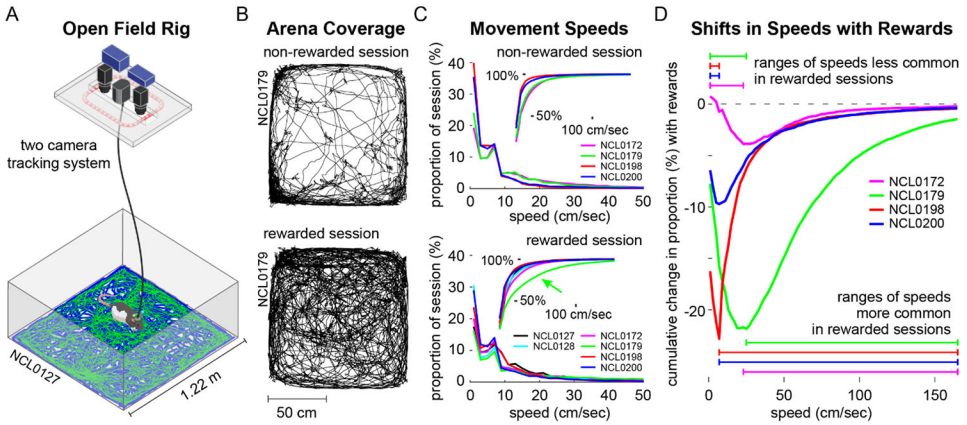

Figure 1. Locomotor behavior during free exploration and foraging.

A. Open field behavioral arena with separate cameras for tracking body contour and head-fixed LEDs. Blue and green traces on the arena floor illustrate representative LED tracking data. **B.** Examples of locomotor paths taken by the same rat during a non-rewarded session (**top**) and a rewarded session (**bottom**). **C.** Speed occupancy during non-rewarded (top) and rewarded sessions (bottom) for each rat. Insets show speed occupancy as cumulative proportions of session time across increasing movement speeds, e.g. rat NCL0179 spent a greater proportion of the rewarded session at faster movement speeds than did the other rats (green arrow). **D.** Changes in speed occupancy between non-rewarded and rewarded sessions, shown as the difference in proportion accumulated across speeds. Negative peaks in these curves reflect the speed below which rats spent less time during rewarded sessions in favor of faster speeds.

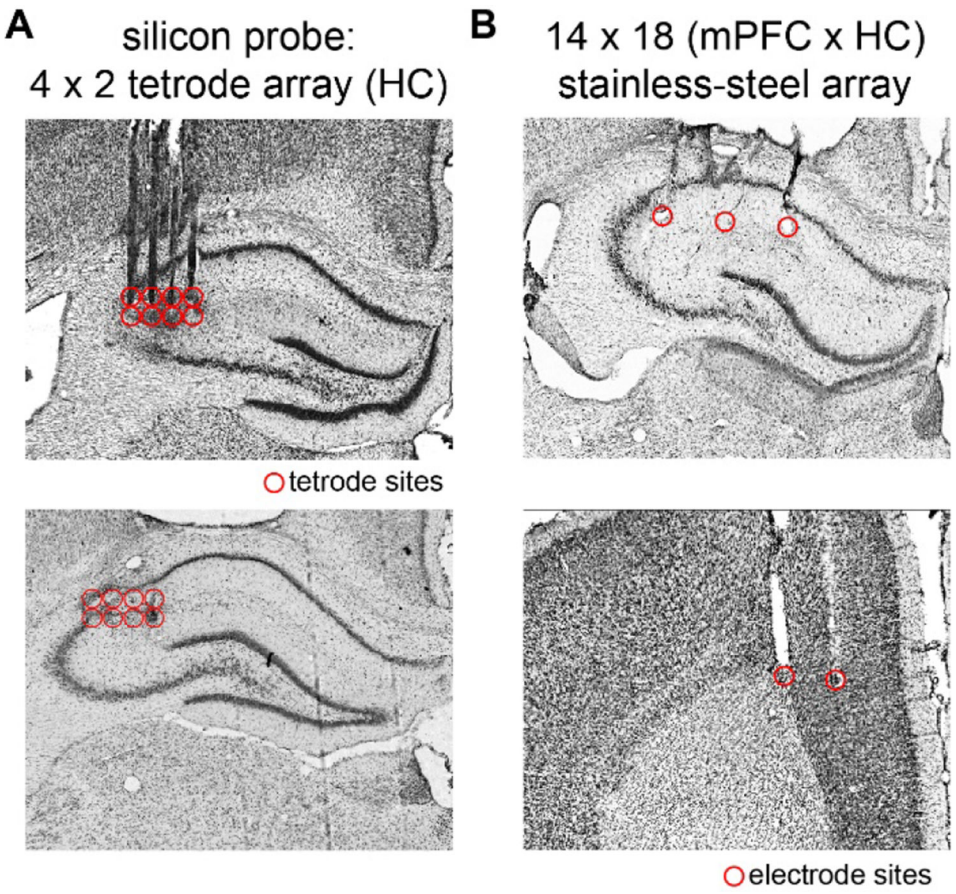

Figure 2. Local field potential recording sites in HC and mPFC.

A. Representative brain slices through HC (**top** and **bottom**) showing tracks left by silicon probe shanks and recording sites (red circles) near the junction of proximal CA1 and CA2.

B. Representative brain slices through HC (**top**) and mPFC (**bottom**) showing stainless steel wire electrode tracks and recording sites.

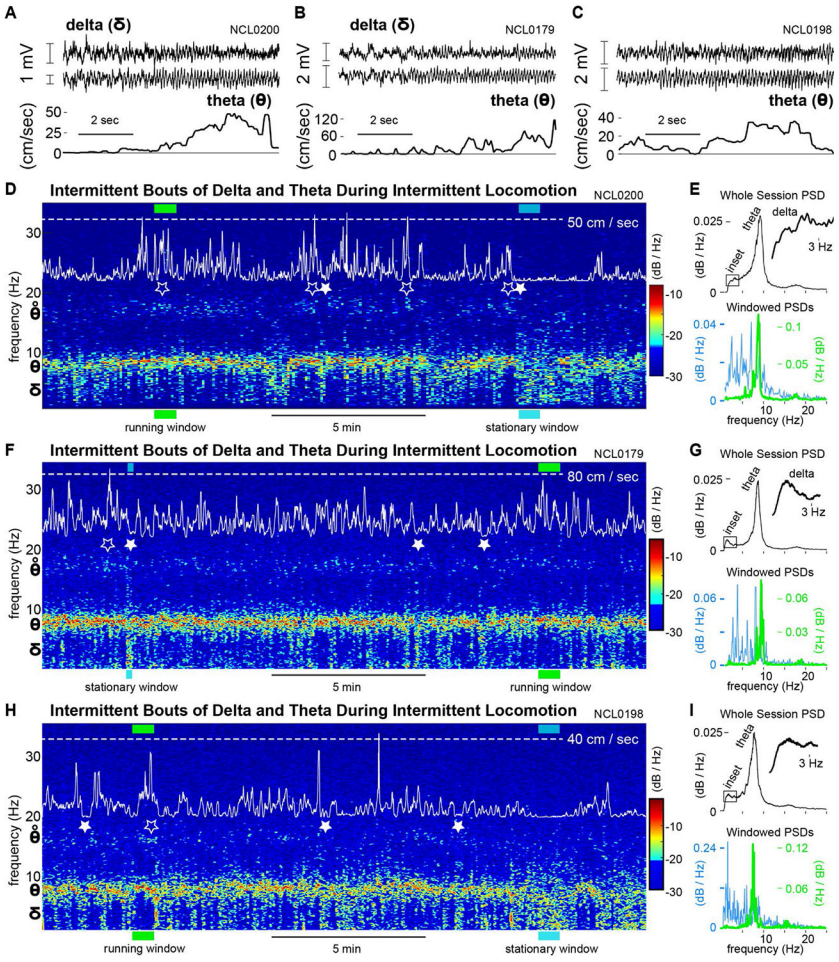

Figure 3. Spectral content of HC LFPs during navigation.

A-C. Pairs of representative, simultaneously recorded HC LFPs (top two traces) and corresponding movement speeds (bottom trace) for three rats. **D.** Spectrogram of the HC LFP showing the theta rhythm (6-10 Hz) prominently throughout the session (warm colors). Movement speed is overlaid on the spectrogram (white trace) to allow comparison of running speed peaks (e.g. open stars, accompanied by theta-harmonic power) and stationary behavior (filled stars) to the spectral content of the LFP. **E.** Power spectral densities for the whole recording session (top) and for representative windows (36 seconds) of running and stationary behavior. Timing of these windows within the recording session is indicated with green and cyan bars in D. **F-I.** As D&E, for two additional rats.

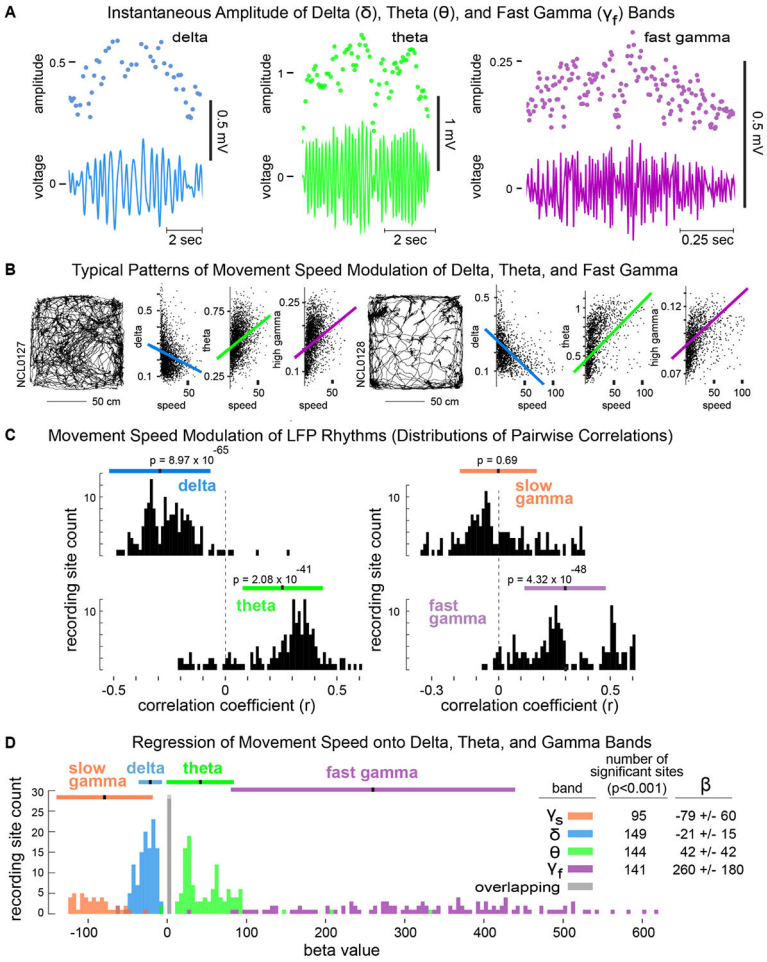

Figure 4. Movement speed modulation of delta, theta, and gamma amplitudes.

A. Instantaneous amplitudes of delta, theta, and gamma were derived from peak-to-trough measurements (dots above) of corresponding band-pass filtered LFPs (voltage traces below). **B.** Scatterplots of instantaneous amplitudes of delta, theta, and high gamma, and overlaid best-linear-fits, corresponding to rats' locomotor trajectories (left) during two representative sessions. **C.** Distributions across all rats and recording sites of pairwise correlation coefficients relating the instantaneous amplitude of each frequency band to movement speed. **D.** Distributions of β-values for significant predictors (p's<0.001) of movement speed from regressions onto instantaneous amplitudes of delta, theta, and slow and fast gamma bands. The inset table shows the number of recording sites for which each band was a significant predictor and the corresponding mean β-values and standard deviations.

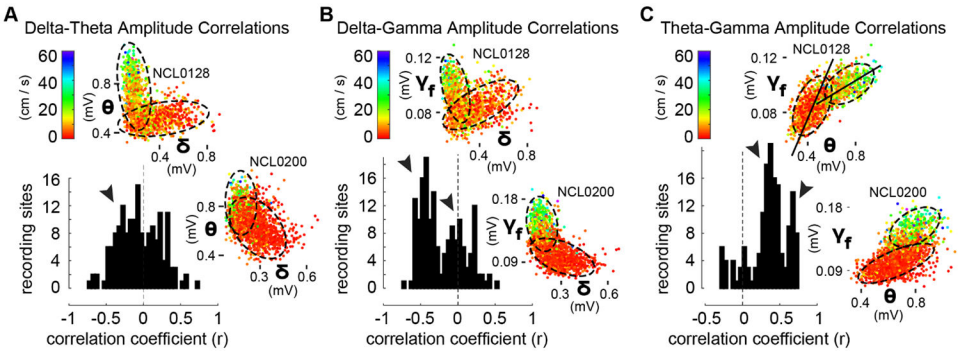

Figure 5. Multimodal distributions of cross-frequency amplitude couplings comprise diverse putative modes.

A. Distribution across HC recording sites of r-values for pairwise correlations between instantaneous amplitudes of delta and theta (black histogram). Scatterplots inset above and at right illustrate for typical orthogonality and anticorrelation between bands, respectively, for one recording site from each of two rats. The weakly-negative histogram peak (arrowhead), merges all individual cases as in the insets. Visually-distinguished delta- and theta-dominated putative modes (dashed ellipses) corresponded to behavioral state (color code for movement speed at top left). **B.** Bimodal distribution of r-values between delta and fast gamma amplitudes (black histogram, arrowheads indicate one prominent negative peak and one peak at zero), and representative scatterplots of delta and fast gamma amplitudes for the same recordings as in insets in A. Orthogonality, and within-mode anticorrelation during running (red mode for rat NCL0200) are evident in visually-defined putative modes (ellipses). **C**. Bimodal distribution of r-values between theta and fast gamma amplitudes (black histogram, arrowheads indicate two prominent positive peaks), and representative scatter plots for the same recordings as in insets in A&B. Insets show globally-positive correlations between theta and fast gamma amplitudes, but these comprise visually-defined putative modes (ellipses) characterized by specific slopes between bands (long axis of ellipses, as in top inset).

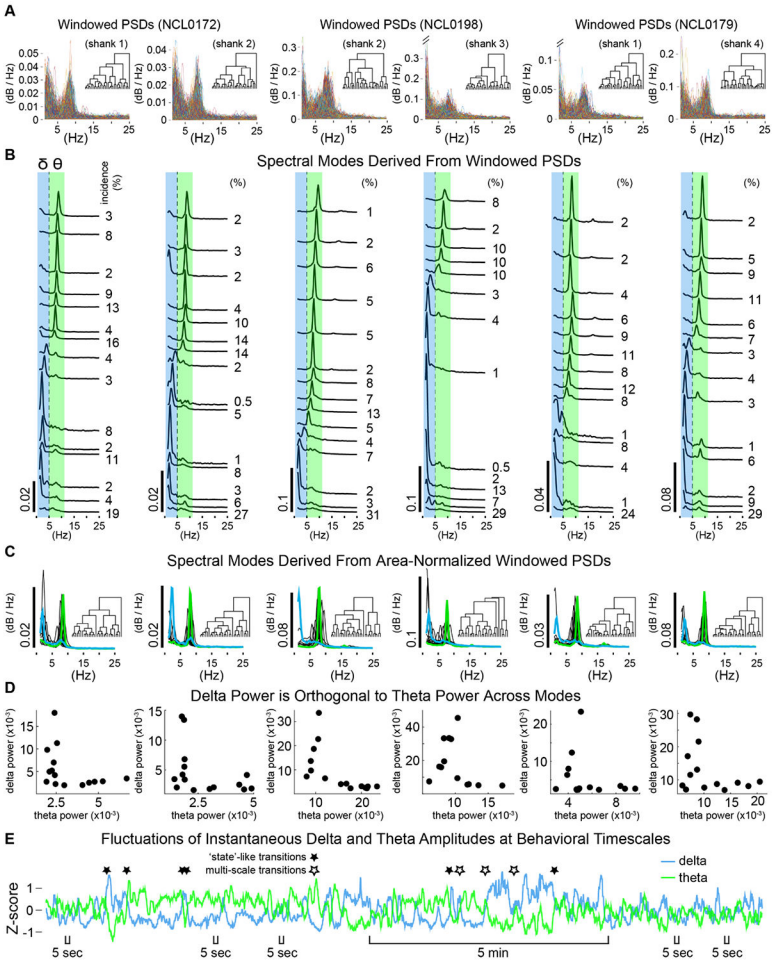

Figure 6. Spectral modes of HC network activity from hierarchical clustering of PSDs.

A. Stacks of all power spectral densities (overlaid) from two second windows of HC LFPs. Examples are shown for two simultaneously recorded channels from each of three rats. Inset dendrograms show the cluster hierarchies. **B.** Spectral modes defined as the average PSD from each cluster of windowed PSDs in A. Larger amplitude modes were primarily evident central to the theta frequency band (green) or within the delta band (blue). The incidence of each mode (% of session) is indicated to the right. **C**. Spectral modes defined conservatively using area-normalized windowed PSDs (dendrograms inset). Representative delta-dominated and theta-dominated modes (average PSDs for example clusters) shown in blue and green, respectively. **D**. Measures of average power within delta and theta frequency bands were orthogonal across modes. Each dot represents delta and theta measures for one mode. **E**. Example time-course of delta and theta showing near-simultaneous fluctuations of the two frequency bands in opposite directions. Several sharp, opposite fluctuations (e.g. filled stars) are consistent with state transitions, but note occasional instances where delta and theta covary (positively) at a fast timescale while diverging over a slower timescale (multi-scale transitions, open stars). Also note that opposite fluctuations in delta and theta can be large or small and take place rapidly. (Five second scale bars indicate a few of many instances where smaller, fast fluctuations in delta and theta directly oppose one another.)

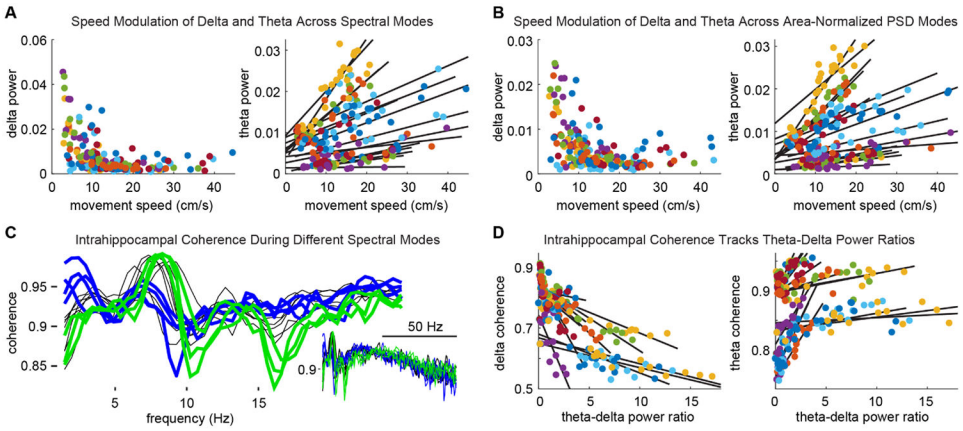

Figure 7. Spectral modes track behavior and network state.

A. Modes with elevated delta power were evident when animals were stationary or moving slowly, whereas modes corresponding to running had minimal delta power (left). In contrast, theta power consistently scaled with running speed across modes. Different colors represent different recording sites across rats (in A, B & D). **B**. Using area-normalized mode definitions, delta and theta power across modes corresponded to animals' movement speeds as in A. **C**. Intrahippocampal coherence spectra for modes from a representative session. Blue traces highlight modes with high delta-frequency coherence and lesser theta coherence. Modes exhibiting high theta coherence between HC recording sites had lesser delta coherence (green traces). **D**. Across modes, delta coherence decreased monotonically (left) and theta coherence increased (right) with increasing theta-delta ratios.

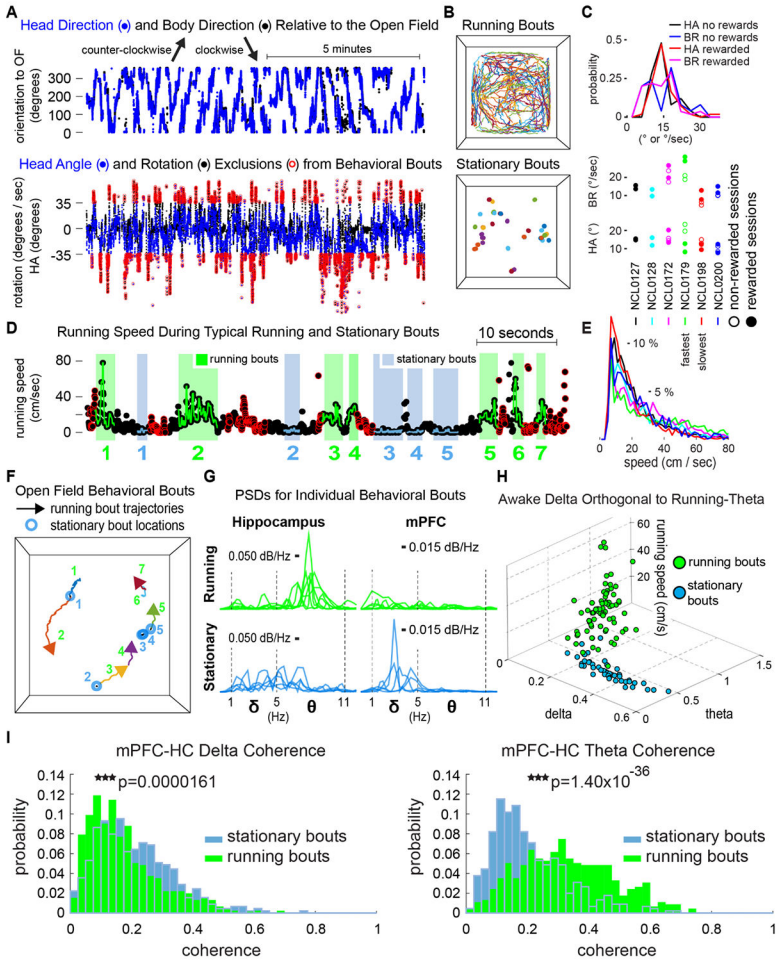

Figure 8. Delta-theta orthogonality and mPFC-HC coherence during intermittent stationary and running bouts.

A. Representative time-course of body direction (black) and head direction (blue) relative to the open field (**top**). Body rotation speed (BR, black) and head angle (HA, blue) (**bottom**). Data points circled in red indicate time stamps excluded from stationary and running bouts, because they exceeded either 52.5 degrees per second of rotational velocity or 35 degrees of head angle. **B.** Locomotor paths during running bouts (top) and locations of stationary bouts in the open field (bottom) for a representative session. **C**. HA and BR incidence (**top**). Mean HA and BR for each rat (**bottom**). **D**. Intermittent stationary (blue) and running bouts (green), after HA and BR exclusions (red circles) and additional restrictive criteria. **E**. Distributions of speeds visited during running bouts for each rat. **F**. Spatial trajectories of bouts in D. **G**. HC and mPFC PSDs for each bout in D. HC PSDs during running bouts exhibit prominent theta peaks, whereas delta power was elevated during stationary bouts, particularly in mPFC. **H**. Delta-theta orthogonality divided stationary from running bouts, whereas theta power covaried with speed across running bouts. **I.** Delta coherence between mPFC and HC increased during stationary bouts, and theta coherence increased during running bouts.